Progress In Electromagnetics Research, PIER 38, 29–45, 2002

BEHAVIOR OF THE REGULARIZED SAMPLING INVERSE SCATTERING METHOD AT INTERNAL RESONANCE FREQUENCIES

N. Shelton and K. F. Warnick

Department of Electrical and Computer Engineering
Brigham Young University
459 Clyde Building, Provo, UT 84602, USA

Abstract—The original proof of the Colton-Kirsch regularized sampling inverse scattering algorithm does not apply at frequencies which are eigenvalues of the interior Helmholtz problem. We explain numerical observations of the behavior of the method and show that useful information about scatterer shape can be obtained at internal resonance frequencies.

1. INTRODUCTION

As computational resources increase in power and numerical algorithms for solving forward electromagnetic scattering problems have improved in efficiency, interest has turned to inverse scattering, or the problem of determining scatterer shape and composition from scattered fields. In the search for more effective inverse scattering algorithms, Colton and Kirsch's regularized sampling method [1, 2] has been touted as a compromise between computationally-expensive nonlinear optimization algorithms and faster, less accurate methods based on linearizing approximations.

The Colton-Kirsch regularized sampling method returns a reconstruction of the region of support of the scatterer from the norm of the solution to a linear integral equation at each pixel point. Unlike optimization methods, regularized sampling does not require a priori information about the scatterer shape or composition. The method has been extended to inhomogeneous media [3] and 3D objects [4] as well as static fields [5, 6]. The mathematical foundations of regularized sampling were investigated further in [7]. Although it is not based on a Born-type single scattering approximation, the method has been shown to suffer from poor reconstruction quality for convex scatterers similar to other methods based on linearizing approximations [8].

One difficulty with regularized sampling is that the proof on which is is based does not apply at eigenvalues of the interior Helmholtz problem, or internal resonances. As the electrical size of a scatterer increases, these resonances become more closely spaced in frequency, so that at high frequencies the likelihood that internal resonance will affect image reconstruction increases. In order to avoid failure of scatterer reconstruction in practical applications, it is important to understand the behavior of the regularized sampling method at or near internal resonances.

In this paper, we show that the reconstructed scatterer image becomes hollow at internal resonance frequencies, and demonstrate numerically that information on scatterer support can still be obtained at resonances. These results may explain internal structure observed in numerical results [8] and lead to improved thresholding approaches for determining scatterer support with regularized sampling. The treatment also provides some insight into unexplained features of regularized sampling, such as behavior of the method outside the scatterer.

We confine attention to the original 2D Colton-Kirsch method in two dimensions [1] with regularization [2] for TM-polarized fields or the exterior Helmholtz problem with Dirichlet boundary condition.

2. REGULARIZED SAMPLING METHOD

Here we review the main features of the regularized sampling method [1, 2]. At each image pixel point $\boldsymbol{\rho}_0$ in the reconstruction domain, the regularized sampling method requires solution of the integral equation

$$\int_0^{2\pi} F_\infty(\phi,\theta) g(\theta,\boldsymbol{\rho}_0) d\theta = e^{-i\mathbf{k}^s\cdot\boldsymbol{\rho}_0} \tag{1}$$

where $F_\infty(\phi,\theta)$ is the scattering amplitude at angle ϕ for a plane wave incident at angle θ and $\mathbf{k}^s$ is a wavevector at angle ϕ. Since the far field data $F_\infty(\phi,\theta)$ is smooth, the integral equation can be discretized by point evaluation of the kernel, leading to the linear system

$$\mathbf{Fg} = \mathbf{f}(\boldsymbol{\rho}_0) \tag{2}$$

where $\mathbf{F}$ is a set of measured scattering amplitudes for a set of scattered angles ϕ_m, $1 \le m \le M$ and incident angles θ_n, $1 \le n \le N$. The theorem on which the method is based dictates that the norm of $g(\theta,\boldsymbol{\rho}_0)$ becomes infinite as $\boldsymbol{\rho}_0$ approaches the scatterer boundary from the inside. The support of the scatterer's exterior surface corresponds to points for which $\|g\|$ becomes large. The theorem does not specify image behavior for points outside the scatterer.

Due to the smoothness of the far field data F_∞, the integral Equation (1) is ill-posed. Because of this, a regularization scheme must be used in order to uniquely specify the solution g. One approach to this is Tikhonov/Morozov regularization [2, 7]. By expressing the SVD of the scattering matrix as $\mathbf{F} = \mathbf{USV}^H$ and letting $\mathbf{u} = \mathbf{U}^H\mathbf{f}$, the norm of the discrete solution $\mathbf{g}$ is given by

$$\|g\|^2 = \sum_{n=1}^{N} \frac{s_n^2}{(\alpha + s_n^2)^2} |u_n|^2 \tag{3}$$

where s_n denotes the singular values S_{nn}. The regularization parameter α is found as the zero of

$$m_A(\alpha) = \sum_{n=1}^{N} \frac{\delta^2 s_n^2 - \alpha^2}{(\alpha + s_n^2)^2} |u_n|^2 \tag{4}$$

where δ is the data error bound such that $\|\mathbf{F} - \mathbf{F}_{\text{exact}}\| < \delta$.

2.1. Alternate Derivation

In order to study the behavior of regularized sampling near internal resonances, we provide an alternate derivation of the integral Equation

(1). Let D be a circle enclosing the scatterer S, and consider the integral equation

$$L_D J = E_D \tag{5}$$

where

$$L_D J = \frac{k\mu}{4} \int_{\partial S} H_0^{(1)}(k|\boldsymbol{\rho} - \boldsymbol{\rho}'|) J(\boldsymbol{\rho}') d\boldsymbol{\rho}', \quad \boldsymbol{\rho} \in D. \tag{6}$$

Here, J is the z component of the surface current on the scatterer ∂S induced by an incident field, and E_D is the corresponding scatterered field evaluated on the circle D. We note that a similar operator was used by Kress used in extending regularized sampling to static fields [5, 6].

We now constrain E_D to be the z component of the electric field radiated by a line source at $\boldsymbol{\rho}_0$, so that

$$E_D(\boldsymbol{\rho}) = E_{\boldsymbol{\rho}_0}(\boldsymbol{\rho}) = H_0^{(1)}(k|\boldsymbol{\rho} - \boldsymbol{\rho}_0|) \tag{7}$$

where $\boldsymbol{\rho}_0$ is a point inside the circle D. In the following, we will refer to the 3D line source as a point source located at $\boldsymbol{\rho}_0$. If $\boldsymbol{\rho}_0$ is inside S, then by Huygens' principle there exists some finite current J on the scatterer which radiates the field E_D, and we have that

$$\|J\| < \infty, \quad \boldsymbol{\rho}_0 \in S \tag{8}$$

where $\|\cdot\|$ denotes the L_2 norm. If $\boldsymbol{\rho}_0$ lies on the scatterer surface ∂S, then also by Huygens' principle the surface current induced on the scatterer is singular, and

$$\|J\| = \infty, \quad \boldsymbol{\rho}_0 \in \partial S. \tag{9}$$

We note that the previous two observations fail at internal resonance frequencies. The ramifications of this are considered in the next section.

It remains to consider the case of the point source lying outside the scatterer. If $\boldsymbol{\rho}_0$ is outside of S, then we have the following simple corrolary of Rellich's lemma [9–11].

Theorem. Assume that D is a circle enclosing a current distribution J defined on the domain $\overline{S}$. Then there is no finite current J on $\overline{S}$ which radiates a field at D equal to that of a point source outside ∂S.

Proof. Let J be a finite current on $\overline{S}$ which radiates a field E_J such that $E_J|_D = E_{\boldsymbol{\rho}_0}|_D$ for some $\boldsymbol{\rho}_0 \notin \overline{S}$. By Huygens' principle, $E_J = E_{\boldsymbol{\rho}_0}$ outside of the circle D. Rellich's lemma states essentially that if a solution to the 2D Helmholtz equation defined outside some ball decays at infinity more rapidly than $\rho^{-1/2}$, then the solution must

vanish identically. Applying Rellich's lemma to the difference $E_J - E_{\boldsymbol{\rho}}$ shows that $E_J(\boldsymbol{\rho}) = E_{\boldsymbol{\rho}}(\boldsymbol{\rho})$ for all $\boldsymbol{\rho}$ not lying on $\overline{S}$ or $\boldsymbol{\rho}_0$.

At the same time, Huygen's principle dictates that E_J must be analytic outside the support of the current J. Thus, $E_{\boldsymbol{\rho}_0}$ can have at most a removable singularity at $\boldsymbol{\rho}_0$, which is a contradiction, as $E_{\boldsymbol{\rho}_0}(\boldsymbol{\rho}) = H_0^{(1)}(k|\boldsymbol{\rho} - \boldsymbol{\rho}_0|)$ does not have a removable singularity at $\boldsymbol{\rho} = \boldsymbol{\rho}_0$.

By making use of this result, we see that $E_D = E_{\boldsymbol{\rho}_0}|_D$ is not in the range of the operator L_D, and therefore

$$\|\mathbf{J}\| \to \infty, \quad \boldsymbol{\rho}_0 \notin \overline{S} \tag{10}$$

We have shown that the solution J in Eq. (5) is finite if $\boldsymbol{\rho}$ is inside ∂S and has infinite norm otherwise.

We now consider the far field limit of (5). By making use of

$$H_0^{(1)}(x) \sim \sqrt{\frac{-2i}{\pi x}} e^{ix}, \quad x \to \infty, \tag{11}$$

Eq. (5) becomes

$$\frac{k\eta}{4} \int_{\partial S} e^{-ik\hat{\rho}\cdot\boldsymbol{\rho}'} J(\boldsymbol{\rho}') d\boldsymbol{\rho}' = e^{-ik\hat{\rho}\cdot\boldsymbol{\rho}_0}. \tag{12}$$

Let E^i be the incident field which produces the current J on the scatterer surface ∂S, and let L be the electric field integral operator defined by

$$LJ = \frac{k\eta}{4} \int_{\partial S} H_0^{(1)}(k|\boldsymbol{\rho} - \boldsymbol{\rho}'|) J(\boldsymbol{\rho}') d\boldsymbol{\rho}', \quad \boldsymbol{\rho} \in \partial S. \tag{13}$$

Using this operator, we can express J in terms of an incident field E^i as

$$J = L^{-1} E^i \tag{14}$$

We now expand E^i as a plane wave spectrum with angular distribution $g(\theta)$, so that

$$E^i(\boldsymbol{\rho}) = \int_0^{2\pi} g(\theta) e^{i\mathbf{k}^i\cdot\boldsymbol{\rho}} d\theta \tag{15}$$

where $\mathbf{k}^i = -\hat{x}k\cos\theta - \hat{y}k\sin\theta$. Combining the previous two equations yields

$$J = L^{-1} \int_0^{2\pi} e^{i\mathbf{k}^i\cdot\boldsymbol{\rho}} g(\theta) d\theta. \tag{16}$$

Substituting this result into Eq. (12) leads to the integral equation

$$\int_0^{2\pi} \left[\frac{k\eta}{4} \int_S d\boldsymbol{\rho}' e^{-i\mathbf{k}^s \cdot \boldsymbol{\rho}'} L^{-1} e^{i\mathbf{k}^i \cdot \boldsymbol{\rho}'} \right] g(\theta) d\theta = e^{-i\mathbf{k}^s \cdot \boldsymbol{\rho}_0} \tag{17}$$

where $\mathbf{k}^s = k\hat{\rho} = \hat{x}k\cos\phi + \hat{y}k\sin\phi$. Recognizing that the scattering amplitude $F_\infty(\phi, \theta)$ in the direction ϕ due to a plane wave incident at angle θ is

$$F_\infty(\phi, \theta) = -\frac{k\eta}{4} < E^s, J > \tag{18}$$

where J is the current induced on the scatterer by the incident plane wave $e^{i\mathbf{k}^i \cdot \boldsymbol{\rho}}$ and the inner product is over the scatterer S, we see that Eq. (17) can be written as

$$\int_0^{2\pi} F_\infty(\phi, \theta) g(\theta) d\theta = e^{-i\mathbf{k}^s \cdot \boldsymbol{\rho}_0} \tag{19}$$

where we absorb a sign into $g(\theta)$. This is Eq. (1).

This derivation of the regularized sampling equation provides a physical interpretation of the method. The function g defines an incident field which on striking the scatterer produces a scattered field equal to that of a point source located at $\boldsymbol{\rho}_0$. The theorem proved above implies that no finite incident field can illuminate the scatter in such a way that the scattered fields appear to emanate from a point source located on or outside the scatterer. This is more general than the usual physical interpretation, which is that this incident field becomes unbounded as the point source approaches the boundary of the scatterer from the inside [12].

Most importantly for the purposes of this paper, the integral equation (5) extends the usual physical interpretation of regularized sampling for the case of the point source located inside the scatterer. In this case, Eq. (5) can be viewed as the extinction theorem for the interior Helmholtz problem for the boundary ∂S. This will be used below to analyze the behavior of the regularized sampling method at internal resonances.

3. INTERNAL RESONANCE FREQUENCIES

At an internal resonance frequency, the Helmholtz equation has a nontrivial solution in the interior of the scatterer which satisfies the Dirichlet boundary condition. Physically, the interior of S has a cavity resonance. The surface current on ∂S corresponding to the resonant mode also is an eigenfunction operator L in Eq. (13) with a zero

eigenvalue. This mode cannot be excited by external fields, but is excited with infinite amplitude by any source inside S that has nonzero coupling with the resonant mode. We now consider the consequences of this observation for the regularized sampling method.

A point source inside S will excite the internal resonant mode unless it is located at a null of the mode's electric field pattern. Thus, if the point source location $\boldsymbol{\rho}_0$ is not at an electric field null, then the current J in Eq. (5) induced on the scatterer surface is infinite. The incident field which produces this same current on ∂S by exterior illumination must be infinite as well, because the surface current due to the resonant mode does not radiate outside S and is in the null spaces of the L and L_D operators. In view of Eq. (15), the norm is infinite in this case.

If the point source is located at a null of the resonant mode, then the source does not excite the mode, and the current J on the scatterer surface is finite. From this we see that $\|g\|$ is infinite inside the scatterer except at mode nulls. As the surface of the scatterer also corresponds to a mode null for the Dirichlet boundary condition considered in this paper, the value of $\|g\|$ is finite on the boundary ∂S of the scatterer as well.

If the point source is located outside the scatterer, the resonant mode is not excited, but the norm of $\|g\|$ is infinite by the theorem proved in the previous section. Thus, the reconstructed image of the scatterer is hollow, and consists of the pattern of nulls of the resonant mode, including the outer boundary of the scatterer.

3.1. Circular Cylinder

To illustrate this result, we consider the case of a circular cylinder of radius a, for which the analytical solution [1]

$$g(\theta) = \sum_{n=-N}^{N} \frac{i^{-n} H_n^{(1)}(ka) J_n(k\rho_0)}{2\pi J_n(ka)} e^{-in\theta} \tag{20}$$

can be obtained. At an internal resonance, $J_m(ka) = 0$ for some integer m. In this case, if ρ_0 is not on the boundary of the scatterer or at a mode null, then the norm of g as given by Eq. (20) is infinite, due to the vanishing denominator in the mth term of the summation. If $\rho_0 = a$, then the norm of g becomes finite, as the vanishing factor appears in both the numerator and denominator. At a mode null $\rho = \rho'$ in the interior of the scatterer, $J_m(k\rho') = 0,\ 0 \le \rho' < a$, and the norm becomes finite there as well.

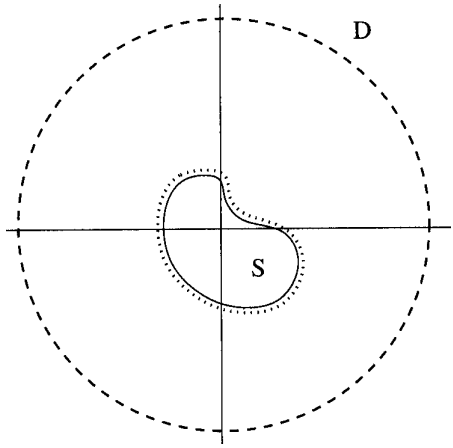

Figure 1. Domain and range of the L_D operator.

4. NUMERICAL RESULTS

The forward scattering data for the simulations in this section was produced by a method of moments solver for the combined field integral equation (CFIE). The CFIE does not become ill-conditioned at internal resonances, so that its use ensures that numerical results are valid at all frequencies. The discretization density was at least 10 unknowns per wavelength to ensure reasonable accuracy in the numerical results. Scattering amplitudes were computed at 64 evenly spaced scattering angles and 64 evenly spaced incident angles.

The matrix error norm used to regularize the solution to Eq. (1) was $\delta = .02$, based on expected numerical error in the forward solver (see [13]). A regularized sampling image is shown in Fig. 2 for reference. As is commonly done, $\|\mathbf{g}\|^{-1}$ is shown, with scale such that lighter pixels represent larger values of $\|\mathbf{g}\|$ and darker pixels smaller values. No image thresholding is done. Figure 2 also shows an image from a linearized tomography method for comparison.

4.1. Near Field Simulations

In order to obtain insight into the behavior of the regularized sampling method, we give numerical solutions to Eq. (5). We discretized the integral equation using the method of moments. The radius of the circle D was chosen to be 10 m, and the radiated electric field was sampled at 64 evenly spaced scattering angles. The desired current values were solved for using the pseudoinverse of $\mathbf{L_D}$ based on the

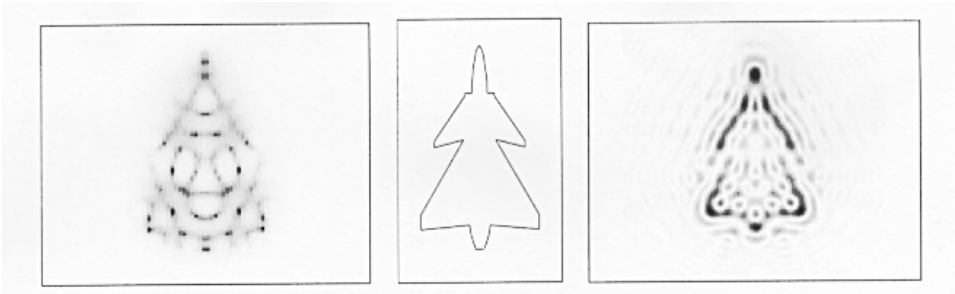

Figure 2. Regularized sampling method (left) and linear tomography method (right). Both images are produced at 100 MHz for the profile of a VFY-218 aircraft.

singular value decomposition. Since $\mathbf{L_D}$ does not represent measured data and error is small, in this case it is sufficient to use a simple spectral cutoff regularization [11], with singular values less than 10^{-12} treated as zero.

Non-resonant case. The first set of simulations consider a 2×1 m rectangular PEC scatterer. The regularized sampling image corresponding to these near field tests is shown in Fig. 3 for reference. Figure 4 shows the computed surface current values and the radiated electric field when $\boldsymbol{\rho}_0 = (0, 0)$, a point inside the scatterer. The scatterer is not resonant at $f = 300$ MHz. Figure 5 shows the current and electric field for $\boldsymbol{\rho}_0 = (0, 1)$, corresponding to an image point outside the scatterer at the same frequency. The current norm becomes very large, as predicted by Eq. (10).

When the point source $\boldsymbol{\rho}_0$ is located on the boundary of the scatterer, the induced surface current is an impulse at at $\boldsymbol{\rho} = \boldsymbol{\rho}_0$ and zero everywhere else. Figure 6 shows the numerical approximation to this singular current obtained for $\boldsymbol{\rho}_0 = (0, 0.5)$ and the electric field radiated by this current. The norm of $\mathbf{J}$ for $\boldsymbol{\rho}_0$ on ∂S is much less than the value obtained for $\boldsymbol{\rho}_0$ outside the scatterer.

Internal resonant case. The 2×1 m rectangle has a TM_{31} mode resonance at $f \approx 270$ MHz. When the point source is located at $\boldsymbol{\rho}_0 = (0, 0)$, large resonant currents are induced on the scatterer, and $\|\mathbf{J}\|$ becomes large even though $\boldsymbol{\rho}_0$ is inside the scatterer. The resulting current and electric field are shown in Fig. 7.

As shown in the previous section, resonance effects produce internal structure in the image. A point source field centered at $\boldsymbol{\rho}_0$ on a null of a particular resonance mode does not excite the resonance current for that mode. At the first three resonance frequencies of the

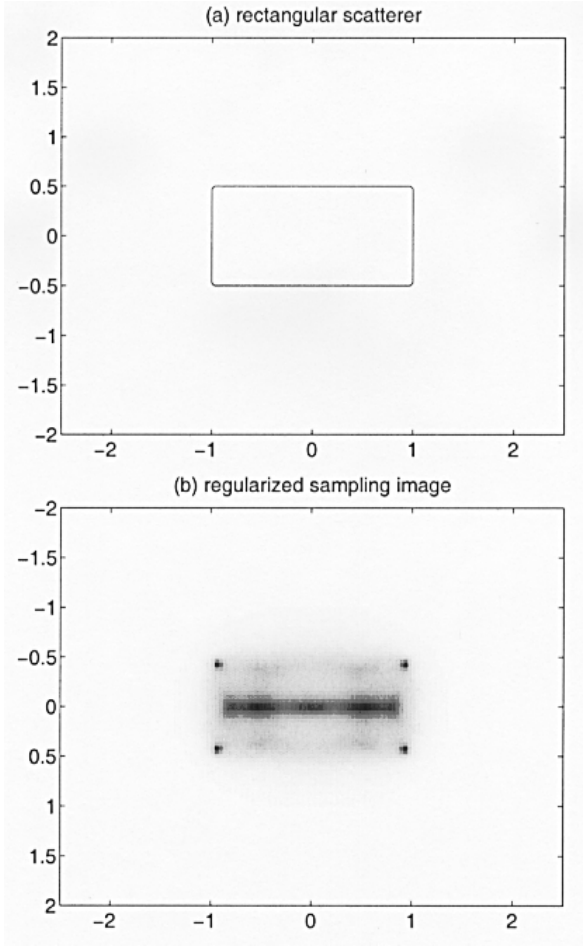

Figure 3. Regularized sampling image for a 2×1 m rectangular scatterer at 300 MHz.

2×1 rectangle in Fig. 8, points corresponding to small values of $\|\mathbf{g}\|$ lie on the electric field nulls of the TM_{11}, TM_{21}, and TM_{31} modes.

4.2. Image Contrast

We now compare a measure of image contrast as a function of frequencies to the inverse condition number of the moment matrix $\mathbf{Z}$ of the electric field integral equation (EFIE). At an internal resonance, the EFIE operator obtains a zero eigenvalue, so that the inverse

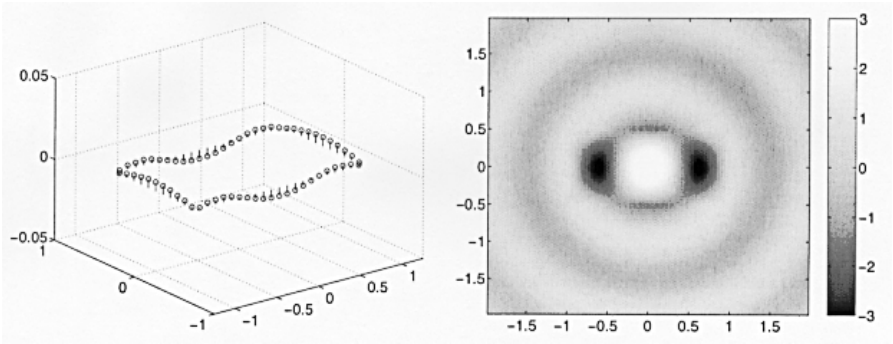

Figure 4. Surface current (left) and radiated electric field (right) for a point source located inside the scatterer at the origin. The frequency is 300 MHz.

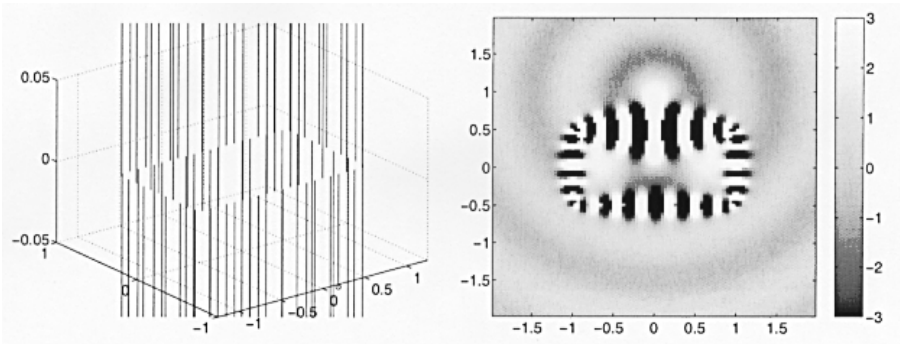

Figure 5. Surface current (left) and radiated electric field (right) for a point source located inside the scatterer at $\boldsymbol{\rho}_0 = (0, 1)$. The frequency is 300 MHz.

condition number becomes small at resonance, and provides a measure of distance to resonance for scatterer shapes for which resonance frequencies are not known analytically. The image contrast is the ratio of the RMS norm of image pixel values inside the scatterer to the norm of image pixel values across the entire reconstruction domain, along a line passing through the scatterer. By the results obtained in this paper, image contrast should decrease at resonances, since the image becomes hollow. Results are shown in Fig. 9 for several convex scatterers, and the expected correlation between inverse condition number and image contrast is observed.

For other scatterers, however, low image contrast does not correlate exactly with internal resonance frequencies. Figure 10

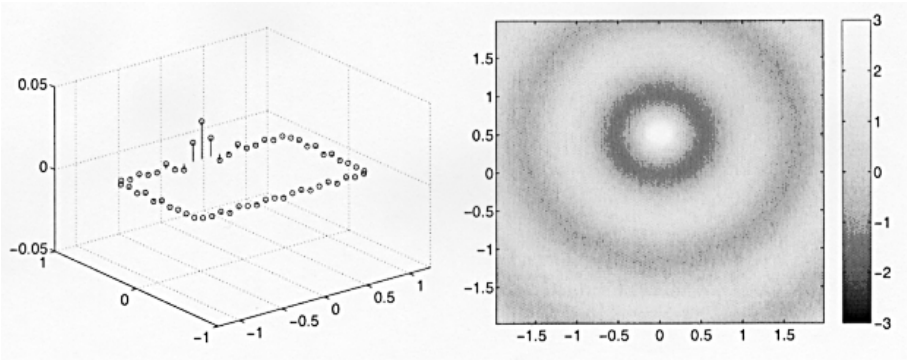

Figure 6. Surface current (left) and radiated electric field (right) for a point source located on the boundary of the scatterer at $\boldsymbol{\rho}_0 = (0, 0.5)$. The frequency is 270 MHz.

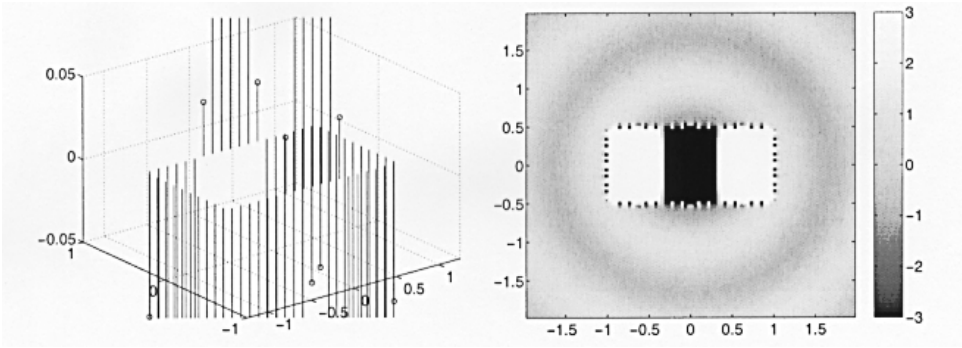

Figure 7. Surface current (left) and radiated electric field (right) for a point source located inside the scatterer at the origin, at an internal resonance (270 MHz).

shows image contrast and EFIE inverse condition number for an L-shaped scatterer and VEY-218 aircraft profile. For these examples, the frequencies of poorest image contrast is shifted slightly from the internal resonance frequencies. It appears that this phenomenon may be associated with the concavity of the scatterers, as the convex hull of the VEY-218 exhibits a much closer correlation between contrast ratio minima and resonance frequencies (Fig. 11). The shifting appears to be independent of regularization parameter, the number of incident and scattered angles at which forward far field data is measured, and the accuracy of the simulated forward data.

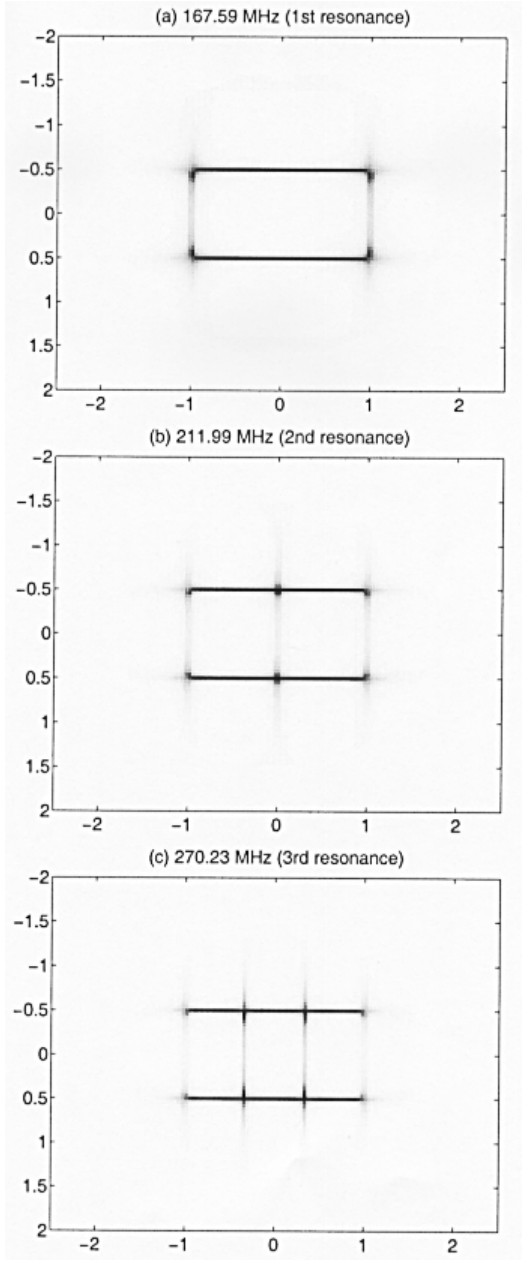

Figure 8. Regularized sampling images at the 1st internal resonance (167.59 MHz), 2nd resonance (211.99 MHz), and 3rd resonance (270.23 MHz). The mode null structure is clearly visible in the image.

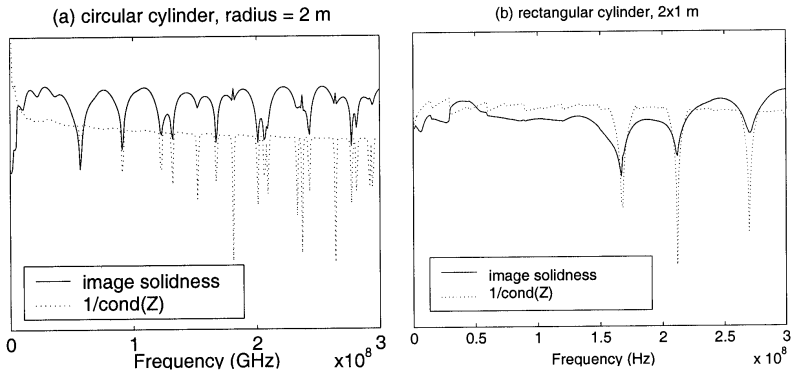

Figure 9. Convex scatterers. Image contrast ratio and the inverse condition number of the discretized electric field integral equation operator as a function of frequency.

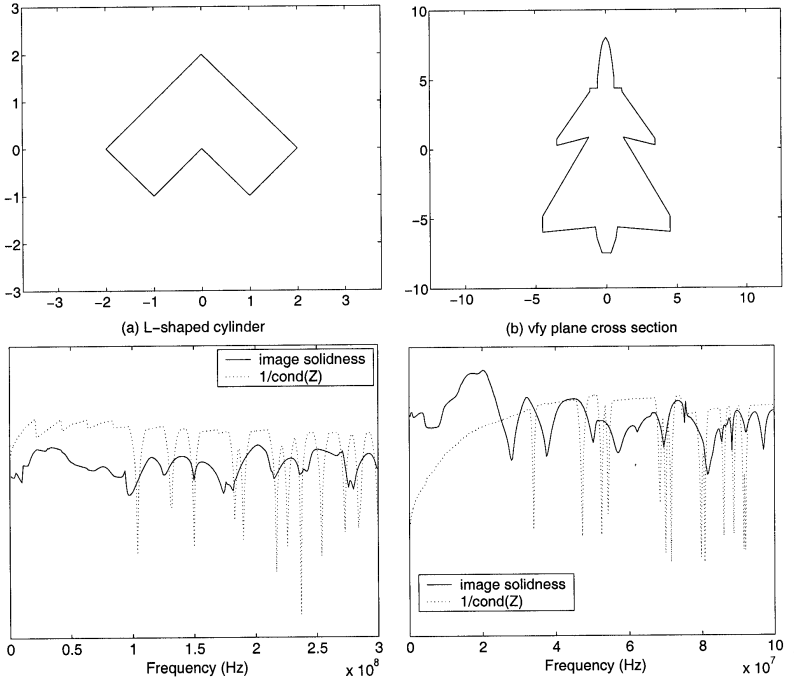

Figure 10. Concave scatterers. Image contrast ratio and the inverse condition number of the discretized electric field integral equation as a function of frequency. Note that contrast minima do not coincide with resonances for these scatterers.

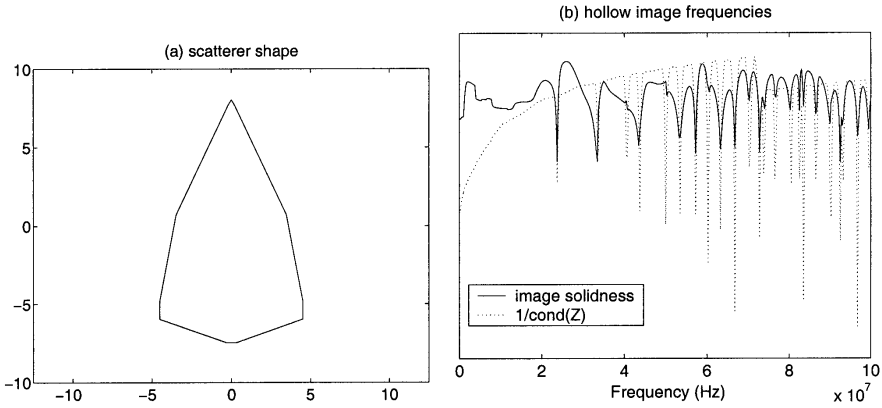

Figure 11. Concave hull of the VEY-218. Image contrast ratio and the inverse condition number of the discretized electric field integral equation as a functions frequency.

5. CONCLUSION

In this paper, we have shown that regularized sampling images correspond to mode null patterns at internal resonance frequencies. This can be explained physically by considering that the norm of the solution to the regularized sampling equation is related to the current excited on the scatterer surface by a point source. At resonance, a point source inside the scatterer excites an infinite current, leading to a "white" or low pixel value for the inverse norm of the current. If the point source is located on a null of the resonant mode, a finite current is excited, and the pixel value is "black" or relatively large.

This predicted behavior is observed in numerical experiments for computed images from simulated scattered field data at low order resonance frequencies. At higher frequencies, strong and complex internal structure is nearly always observed (e.g., Fig. 2). We conjecture that this structure is due to the same effect but for higher order near-resonances with complex null patterns. These results indicate that information on scatterer support can still be obtained at internal resonance frequencies by taking large image pixel values as the scatterer's outer contour instead of the thresholding usually employed.

Computation of an image contrast measure as a function of frequency indicates that these hollow images lead to minima in the image contrast at resonance frequencies. For some concave scatterers, the contrast minima do not coincide exactly with resonances. This

behavior is as yet unexplained.

Finally, the results of this paper also indicate a possible reason that regularized sampling images appear to suffer from degradation for concave regions of a scatterer, similar to linearized methods such as those based on the Born approximation that neglect multiple scattering effects. Although the theorem proved in this paper dictates that the norm of the solution to the regularized sampling equation becomes infinite even for a point source location inside a concave region, surface currents on concave regions can more easily radiate fields that appear to emanate from a point source inside the region than is the case for point sources far from the scatterer. While this observation is physically quite intuitive, a quantitative statement would require a study of the asymptotic spectral properties of the L_D operator employed in this paper.

ACKNOWLEDGMENT

We express gratitude to Michael Brandfass for providing a linearized tomography comparison image and Aaron Lanterman for scatterer shape definitions.

REFERENCES

1. Colton, D. and A. Kirsch, "A simple method for solving inverse scattering problems in the resonance region," *Inverse Problems,* Vol. 12, 383–393, 1996.
2. Colton, D., M. Piana, and R. Potthast, "A simple method using Morozov's discrepancy principle for solving inverse scattering problems," *Inverse Problems*, Vol. 13, 1477–1493, 1997.
3. Colton, D. and P. Monk, "A linear sampling method for the detection of leukemia using microwaves," *SIAM J. Applied Math.,* Vol. 58, 926–941, 1998.
4. Colton, D., K. Giebermann, and P. Monk, "A regularized sampling method for solving three dimensional inverse scattering problems," *SIAM J. Sci. Comp.,* Vol. 21, No. 6, 2316–2330, 2000.
5. Kress, R. and L. Kuhn, "Linear sampling methods for inverse boundary value problems in potential theory," *Appl. Numer. Math.,* Vol. 43, 143–155, 2002.
6. Kress, R., "A sampling method for an inverse boundary value problem for harmonic vector fields," *III-Posed and Inverse Problems*, S. I. Kabanikhin and V. G. Romanov (eds.), 243–262, VSP, Utrecht, 2002.

7. Kirsch, A., "Characterization of the shape of the scattering obstacle using the spectral data," *Inverse Problems*, Vol. 14, 1489–1512, 1998.
8. Brandfass, M., A. Lanterman, and K. Warnick, "A comparison of the Colton-Kirsch inverse scattering method with linearized tomographic inverse scattering," *Inverse Problems,* Vol. 17, 1797–1816, Dec. 2001.
9. Colton, D. and R. Kress, *Integral Equation Methods in Scattering Theory,* John Wiley & Sons, 1983.
10. Lax, P. and R. Phillips, *Scattering Theory,* Revised Edition, Academic Press, Inc., 1989.
11. Colton, D. and R. Kress, *Inverse Acoustic and Electromagnetic Scattering Theory,* Springer, Berlin, 1992.
12. Kress, R., "Uniqueness in inverse obstacle scattering for electromagnetic wave," *Proceedings of the URSI General Assembly,* 2002.
13. Warnick, K. F. and W. C. Chew, "Error analysis of surface integral equation methods," *Fast and Efficient Algorithms in Computational Electromagnetic*, W. C. Chew, J. Jin, E. Michielssen, and J. Song (eds.), 203–282, Artech House, Boston, MA, 2001.